

# Tracking Advanced Planetary Systems (TAPAS) with HARPS-N. V. ★

★★

## A Massive Jupiter orbiting the very low metallicity giant star BD+03 2562 and a possible planet around HD 103485.

E. Villaver<sup>1</sup>, A. Niedzielski<sup>2</sup>, A. Wolszczan<sup>3,4</sup>, G. Nowak<sup>5,6,2</sup>, K. Kowalik<sup>7</sup>, M. Adamów<sup>8,2</sup>, G. Maciejewski<sup>2</sup>, B. Deka-Szymankiewicz<sup>2</sup>, and J. Maldonado<sup>9</sup>

<sup>1</sup> Departamento de Física Teórica, Universidad Autónoma de Madrid, Cantoblanco 28049 Madrid, Spain. e-mail: Eva.Villaver@uam.es

<sup>2</sup> Toruń Centre for Astronomy, Faculty of Physics, Astronomy and Applied Informatics, Nicolaus Copernicus University in Toruń, Grudziadzka 5, 87-100 Toruń, Poland. e-mail: Andrzej.Niedzielski@umk.pl

<sup>3</sup> Department of Astronomy and Astrophysics, Pennsylvania State University, 525 Davey Laboratory, University Park, PA 16802, USA

<sup>4</sup> Center for Exoplanets and Habitable Worlds, Pennsylvania State University, 525 Davey Laboratory, University Park, PA 16802, USA.

<sup>5</sup> Instituto de Astrofísica de Canarias, E-38205 La Laguna, Tenerife, Spain.

<sup>6</sup> Departamento de Astrofísica, Universidad de La Laguna, E-38206 La Laguna, Tenerife, Spain.

<sup>7</sup> National Center for Supercomputing Applications, University of Illinois, Urbana-Champaign, 1205 W Clark St, MC-257, Urbana, IL 61801, USA

<sup>8</sup> McDonald Observatory and Department of Astronomy, University of Texas at Austin, 2515 Speedway, Stop C1402, Austin, Texas, 78712-1206, USA.

<sup>9</sup> INAF - Osservatorio Astronomico di Palermo, Piazza del Parlamento 1, I-90134 Palermo, Italy

Received;accepted

### ABSTRACT

**Context.** We present two evolved stars (HD 103485 and BD+03 2562) from the TAPAS (Tracking Advanced Planetary Systems) with HARPS-N project devoted to RV precision measurements of identified candidates within the PennState - Toruń Centre for Astronomy Planet Search.

**Aims.** Evolved stars with planets are crucial to understand the dependency of the planet formation mechanism on the mass and metallicity of the parent star and to study star-planet interactions.

**Methods.** The paper is based on precise radial velocity (RV) measurements. For HD 103485 we collected 57 epochs over 3317 days with the Hobby-Eberly Telescope and its High Resolution Spectrograph and 18 ultra-precise HARPS-N data over 919 days. For BD+03 2562 we collected 46 epochs of HET data over 3380 days and 19 epochs of HARPS-N data over 919 days.

**Results.** We present the analysis of the data and the search for correlations between the RV signal and stellar activity, stellar rotation and photometric variability. Based on the available data, we interpret the RV variations measured in both stars as Keplerian motion. Both stars have masses close to Solar ( $1.11 M_{\odot}$  HD 103485 and  $1.14 M_{\odot}$  BD+03 2562), very low metallicities ( $[Fe/H] = -0.50$  and  $-0.71$  for HD 103485 and BD+03 2562), and, both have Jupiter planetary mass companions ( $m_2 \sin i = 7$  and  $6.4 M_J$  for HD 103485 and BD+03 2562 resp.), in close to terrestrial orbits (1.4 au HD 103485 and 1.3 au BD+03 2562), with moderate eccentricities ( $e = 0.34$  and  $0.2$  for HD 103485 and BD+03 2562). However, we cannot totally exclude that the signal in the case of HD 103485 is due to rotational modulation of active regions.

**Conclusions.** Based on the current data, we conclude that BD+03 2562 has a bona fide planetary companion while for HD 103485 we cannot totally exclude that the best explanation for the RV signal modulations is not the existence of a planet but stellar activity. If, the interpretation remains that both stars have planetary companions they represent systems orbiting very evolved stars with very low metallicities, a challenge to the conditions required for the formation of massive giant gas planets.

**Key words.** stars: evolution – planets and satellites: individual: HD 103485 and BD+03 2562 – planet-star interactions – stars: late-type

### 1. Introduction

With the discovery of 51 Peg (Mayor & Queloz 1995) we arrived to the realisation that planet formation as we understood it had to

Spanish Observatorio del Roque de los Muchachos of the Instituto de Astrofísica de Canarias.

\* Based on observations obtained with the Hobby-Eberly Telescope, which is a joint project of the University of Texas at Austin, the Pennsylvania State University, Stanford University, Ludwig-Maximilians-Universität München, and Georg-August-Universität Göttingen.

\*\* Based on observations made with the Italian Telescopio Nazionale Galileo (TNG) operated on the island of La Palma by the Fundación Galileo Galilei of the INAF (Istituto Nazionale di Astrofisica) at the

be revised to account for the existence of "Hot Jupiters". Since then, every planetary system discovered has added to our understanding of the physics of planet formation (see e.g. Udry & Santos 2007). In this regard, planets orbiting evolved stars hold the key to several processes related not only to how planet formation operates around stars more massive than the Sun but also to understand star-planet interactions (Villaver & Livio 2007; Villaver et al. 2014; Privitera et al. 2016c,a). In this context, planets around evolved stars have revealed a lack of hot Jupiters that most likely reflect effects induced by stellar evolution (Villaver & Livio 2009; Mustill & Villaver 2012; Villaver et al. 2014; Privitera et al. 2016b).

In the main sequence, the presence of giant planets has shown to be very sensitive to the metallicity [Fe/H] of the host star (Gonzalez 1997; Santos et al. 2004; Fischer & Valenti 2005). The precise functional form of the correlation still remain elusive, despite the fact it is one of the fundamental parameters to help constrain the planet formation models (see e.g. Mordasini et al. 2012). But most important, the evolved hosts of planets have shown to present some chemical peculiarities with respect to their main sequence counterparts (see e.g. Pasquini et al. 2007; da Silva et al. 2006; Ghezzi et al. 2010; Maldonado et al. 2013; Mortier et al. 2013; Jofré et al. 2015; Jones et al. 2014; Reffert et al. 2015; Maldonado & Villaver 2016). In particular, the planet occurrence rate does seem to depend on both stellar mass and stellar metallicity (Maldonado et al. 2013) and cannot be explained by sample contamination (Maldonado & Villaver 2016) as it has been argued by Reffert et al. (2015).

The established picture of giant planet formation, the basis of the core accretion model (Perri & Cameron 1974; Cameron 1978; Mizuno 1980; Pollack et al. 1996), begins with the building of km-sized or larger planetesimals from the growth of 1–10 mm pebbles (see e.g. Youdin 2011; Simon et al. 2016). The planetesimals growth continues until a solid core, big enough for gravity to accrete gas from the protoplanetary disk, is formed. The metallicity dependency in the core accretion model thus comes from the need of a fast core growth before disk dissipation occurs (Ida & Lin 2004). Furthermore, it has been shown that the alternative scenario, giant planet formation via gravitational instability in the protoplanetary disk (Boss 1997; Mayer et al. 2002; Boss 2004) does not carry a metallicity dependency that can explain the observed relation.

Over the last  $\approx 10$  years we have embarked in a quest for substellar/planetary companions to giant stars that started with the PennState - Toruń Centre for Astronomy Planet Search (PTPS, Niedzielski et al. 2007; Niedzielski & Wolszczan 2008; Niedzielski et al. 2015c, 2016a) program and has continued with the high precision RV follow up of previous selected PTPS candidates program Tracking Advanced Planetary Systems (TAPAS) program with HARPS-N (Niedzielski et al. 2015a; Adamów et al. 2015; Niedzielski et al. 2016b,c). In this paper, we present the latest finding of our TAPAS program: two very evolved giant stars with very low metallicities that host a massive "warm" Jupiters and a possible one and thus represent rather extreme outliers to the general planet-metallicity relation.

The paper is organised as follows: a summary of the observations, radial velocity and activity measurements is given in Section 2 together with a description of the general procedure and the basic properties of the two stars; in Section 3 and 4 we show the analysis of the stellar rotation and photometry together with a discussion of the activity indicators; in Section 5 we present the Keplerian analysis of the radial velocity measurements, and our results are summarised and further discussed in Section 6.

**Table 1.** Summary of the available data on HD 103485

| Parameter   | value                  | reference               |
|---|------------------------|-------------------------|
| $V$ [mag]   | $8.28 \pm 0.01$        | Høg et al. (2000)       |
| $B - V$ [mag]   | $1.56 \pm 0.03$        | Høg et al. (2000)       |
| $(B - V)_0$ [mag]                                     | 1.395                  | Zieliński et al. (2012) |
| $M_V$ [mag]   | -2.51                  | Zieliński et al. (2012) |
| $T_{\text{eff}}$ [K]                                  | $4097 \pm 20$          | Zieliński et al. (2012) |
| $\log g$  | $1.93 \pm 0.08$        | Zieliński et al. (2012) |
| [Fe/H]  | $-0.50 \pm 0.09$       | Zieliński et al. (2012) |
| RV [km s <sup>-1</sup> ]                              | $27.56 \pm 0.08$       | Zieliński et al. (2012) |
| $v_{\text{rot}} \sin i_{\star}$ [km s <sup>-1</sup> ] | $2.9 \pm 0.4$          | Adamów et al. (2014)    |
| $A(\text{Li})$  | -0.84                  | Adamów et al. (2014)    |
| [O/H]   | $-0.40 \pm 0.31$       | Adamów et al. (2014)    |
| [Mg/H]  | $-0.27 \pm 0.15$       | Adamów et al. (2014)    |
| [Al/H]  | $-0.10 \pm 0.09$       | Adamów et al. (2014)    |
| [Ca/H]  | $-0.54 \pm 0.18$       | Adamów et al. (2014)    |
| [Ti/H]  | $-0.07 \pm 0.25$       | Adamów et al. (2014)    |
| $M/M_{\odot}$   | $1.11 \pm 0.21$        | Adamczyk et al. (2016)  |
| $\log L/L_{\odot}$                                    | $2.51 \pm 0.13$        | Adamczyk et al. (2016)  |
| $R/R_{\odot}$   | $27.37 \pm 6.69$       | Adamczyk et al. (2016)  |
| $\log \text{age}$ [yr]                                | $9.79 \pm 0.25$        | Adamczyk et al. (2016)  |
| $d$ [pc]  | $1134 \pm 145$         | calculated from $M_V$   |
| $V_{\text{osc}}$ [m s <sup>-1</sup> ]                 | $68.2^{+52.1}_{-28.2}$ | this work               |
| $P_{\text{osc}}$ [d]                                  | $2.2^{+2.0}_{-1.1}$    | this work               |
| $P_{\text{rot}} / \sin i_{\star}$ [d]                 | $477 \pm 134$          | this work               |

## 2. Observations, radial velocities, line bisectors and activity indicators

HD 103485 (BD+02 2493) and BD+03 2562 (TYC 0276-00507-1) belong to a sample of about 300 planetary or brown dwarf (BD) candidates identified from a sample of about 1000 stars searched for radial velocity (RV) variations with the 9.2m Hobby-Eberly Telescope (HET, Ramsey et al. 1998). The full sample have been monitored since 2004 using the High-Resolution Spectrograph (HRS, Tull 1998) at HET within the PTPS program. Targets were selected for a more intense precise RV follow-up within the TAPAS program with the High Accuracy Radial velocity Planet Searcher in the North hemisphere (HARPS-N, Cosentino et al. 2012).

The spectroscopic observations presented in this paper are thus a combination of data taken with the HRS at HET in the queue scheduled mode (Shetrone et al. 2007), and with HARPS-N at the 3.58 meter Telescopio Nazionale Galileo (TNG).

For HET HRS spectra we use a combined gas-cell (Marcy & Butler 1992; Butler et al. 1996), and cross-correlation (Queloz 1995; Pepe et al. 2002) method for precise RV and spectral bisector inverse slope (BIS) measurements, respectively. The implementation of this technique to our data is described in Nowak (2012) and Nowak et al. (2013).

HARPS-N radial velocity measurements and their uncertainties as well as BIS measurements were obtained with the standard user pipeline, which is based on the weighted CCF method (Fellgett 1955; Griffin 1967; Baranne et al. 1979; Queloz 1995; Baranne et al. 1996; Pepe et al. 2002), using the simultaneous Th-Ar calibration mode of the spectrograph and the K5 cross-correlation mask.

A summary of the available data for HD 103485 and BD+03 2562 is given in Tables 1 and 2 respectively.

**Table 2.** Summary of the available data on BD+03 2562

| Parameter   | value                   | reference               |
|---|-------------------------|-------------------------|
| $V$ [mag]   | $9.58 \pm 0.01$         | Høg et al. (2000)       |
| $B - V$ [mag]   | $1.27 \pm 0.09$         | Høg et al. (2000)       |
| $(B - V)_0$ [mag]                                     | 1.38                    | Zieliński et al. (2012) |
| $M_V$ [mag]   | -2.51                   | Zieliński et al. (2012) |
| $T_{\text{eff}}$ [K]                                  | $4095 \pm 20$           | Zieliński et al. (2012) |
| $\log g$  | $1.89 \pm 0.10$         | Zieliński et al. (2012) |
| [Fe/H]  | $-0.71 \pm 0.09$        | Zieliński et al. (2012) |
| RV [km s <sup>-1</sup> ]                              | $50.88 \pm 0.06$        | Zieliński et al. (2012) |
| $v_{\text{rot}} \sin i_{\star}$ [km s <sup>-1</sup> ] | $2.7 \pm 0.3$           | Adamów et al. (2014)    |
| $A(\text{Li})$  | -0.56                   | Adamów et al. (2014)    |
| [O/H]   | $-0.23 \pm 0.22$        | Adamów et al. (2014)    |
| [Mg/H]  | $-0.01 \pm 0.13$        | Adamów et al. (2014)    |
| [Al/H]  | $-0.21 \pm 0.10$        | Adamów et al. (2014)    |
| [Ca/H]  | $-0.68 \pm 0.18$        | Adamów et al. (2014)    |
| [Ti/H]  | $-0.34 \pm 0.24$        | Adamów et al. (2014)    |
| $M/M_{\odot}$   | $1.14 \pm 0.25$         | Adamczyk et al. (2016)  |
| $\log L/L_{\odot}$                                    | $2.70 \pm 0.14$         | Adamczyk et al. (2016)  |
| $R/R_{\odot}$   | $32.35 \pm 8.82$        | Adamczyk et al. (2016)  |
| $\log \text{age}$ [yr]                                | $9.72 \pm 0.28$         | Adamczyk et al. (2016)  |
| $d$ [pc]  | $2618 \pm 564$          | calculated from $M_V$   |
| $V_{\text{osc}}$ [m s <sup>-1</sup> ]                 | $102.9^{+89.9}_{-45.4}$ | this work               |
| $P_{\text{osc}}$ [d]                                  | $2.9^{+2.0}_{-1.1}$     | this work               |
| $P_{\text{rot}}/\sin i_{\star}$ [d]                   | $606 \pm 179$           | this work               |

### 2.1. RV and BIS

The 57 epochs of HET/HRS data for HD 103485 show RV variations of  $553 \text{ m s}^{-1}$  with average uncertainty of  $5.6 \text{ m s}^{-1}$  and BIS variations of  $104 \text{ m s}^{-1}$  with an average uncertainty of  $16 \text{ m s}^{-1}$ . No correlation between RV and BIS exists (Pearson's  $r=0.09$ ). HARPS-N RV 18 epochs of data show an amplitude of  $553 \text{ m s}^{-1}$  (average uncertainty of  $1.7 \text{ m s}^{-1}$ ). The BIS shows a peak-to-peak amplitude of  $85 \text{ m s}^{-1}$  and no correlation with RV ( $r=-0.02$ ). Lomb-Scargle (LS) periodogram analysis (Lomb 1976; Scargle 1982; Press et al. 1992) of combined HET/HRS and HARPS-N RV data reveals a strong periodic signal in RV at 557 days.

For BD+03 2562 the 46 epochs of HET/HRS data show RV variations of  $575 \text{ m s}^{-1}$  with average uncertainty of  $7 \text{ m s}^{-1}$  and BIS variations of  $136 \text{ m s}^{-1}$  with average uncertainty of  $22 \text{ m s}^{-1}$ . The 19 epochs of HARPS-N data show RV amplitude of  $444 \text{ m s}^{-1}$  and average uncertainty of  $2.1 \text{ m s}^{-1}$ . The BIS shows a peak-to-peak amplitude of  $58 \text{ m s}^{-1}$ . There is no correlation between RV and BIS in either HET/HRS data ( $r=0.23$ ) or HARPS-N ( $r=0.13$ ) data. A strong periodic signal in RV at 482 days appears in the LS periodogram analysis of combined HET/HRS and HARPS-N RV data.

HET/HRS and HARPS-N BIS have to be considered separately due to their different definition (see Niedzielski et al. 2016b for more details). The RV and BIS data for both stars are presented in Tables 5, 7, 6 and 8.

### 2.2. Activity indicators: the Ca H&K lines

The Ca II H, and K line profiles (see Noyes et al. 1984; Duncan et al. 1991) and the reversal profile, typical for active stars (Eberhard & Schwarzschild 1913) are widely accepted as stellar activity indicators. The Ca II H and K lines are only available to us in the TNG HARPS-N spectra. The signal-to-noise of our red giants in that spectral range is low, 3-5 in this particular case,

but we found no trace of reversal. To quantify the observations, we calculated an instrumental  $S_{\text{HK}}^{\text{inst}}$  index according to the prescription of Duncan et al. (1991) for HARPS-N data. The  $S_{\text{HK}}^{\text{inst}}$  index for TNG HARPS-N spectra was calibrated to the Mt Wilson scale with the formula given by Lovis et al. (2011). For HD 103485, we obtained a value of  $0.20 \pm 0.05$  and for BD+03 2562 of  $0.14 \pm 0.07$ , rather typical values for non-active stars.

The  $S_{\text{HK}}^{\text{inst}}$  for both stars show no statistically significant correlation with the RV ( $r = -0.41$  and  $r = -0.25$ , respectively). In order to dig deeper into the possible correlation we have performed further statistical Bayesian tests following the prescription given in Figueira et al. (2016). For HD 103485 the Pearson's coefficient of the data is 0.408 with a 0.093 2-sided p-value and the Spearman's rank coefficient is 0.514 (0.029 2-sided p-value). The distribution of the parameter of interest,  $\rho$ , characterizing the strength of the correlation is 0.327 with a standard deviation of 0.187 and 95% credible interval [-0.049 0.663]. For BD+03 2562 the Pearson's coefficient is 0.254, 0.310 2-sided p-value and the Spearman's rank coefficient 0.051 with a 0.841 2-sided p-value.  $\rho = 0.2$  with a 0.197 and 95% credible interval [-0.201 0.559]. For both stars a correlation is not conclusively seen and seems unlikely, with the 95% credible interval lower limit being above  $\rho = 0$ . However, a note of warning is in place here given that in the case of rotational modulation, it is expected to have non-linear relations between RV and activity. This is caused by a phase shift between the activity maximum (that occurs when the active regions are at the centre of the disk) and the maximum RV effect, that happens at a phase of  $\approx 60^\circ$ .

Thus, we conclude that the Ca II H and K line profile analysis reveals that, over the period covered by TNG observations, both giants are quite inactive and there is no trace of activity influence upon the observed RV variations.

### 2.3. Activity indicators: H $\alpha$ analysis

Cincunegui et al. (2007) showed that the calcium and hydrogen lines indices do not always correlate and cannot be used interchangeably as activity indicators. We thus measured the H $\alpha$  activity index ( $I_{H\alpha}$ ) in both HET/HRS and TNG/HARPS-N spectra, following the procedure described in detail by Maciejewski et al. (2013), which based on the approach presented by Gomes da Silva et al. (2012) and Robertson et al. (2013, and references therein). We also measured the index in the Fe I 6593.883 Å control line ( $I_{Fe}$ ) which is insensitive to stellar activity to take possible instrumental effects into account. Moreover, in the case of HET/HRS spectra, that may still contain weak I<sub>2</sub> lines in the wavelength regime relevant to the H $\alpha$  and Fe I 6593.883 Å lines, we also measured the H $\alpha$  and Fe I indices for the iodine flat-field spectra ( $I_{I_2, H\alpha}$  and  $I_{I_2, Fe}$  respectively).

#### 2.3.1. BD+03 2562

The marginal rms variations of the  $I_{I_2, H\alpha} = 0.11\%$  and  $I_{I_2, Fe} = 0.33\%$  in comparison to the relative scatter of  $I_{H\alpha, HRS} = 3.03\%$  and  $I_{Fe, HRS} = 1.08\%$  assure us of the negligible contribution of the weak iodine lines to H $\alpha$  and Fe I 6593.883 Å line indices measured from HET/HRS spectra of BD+03 2562. The rms variation of H $\alpha$  activity index measured from 18 TNG/HARPS-N spectra is slightly larger than the one measured from the HET/HRS spectra ( $I_{H\alpha, HARPS-N} = 3.68\%$ ). The rms variation of TNG/HARPS-N Fe I 6593.883 Å line index is more than two times larger than that measured from HET/HRS spectra ( $I_{Fe, HARPS-N} = 2.39\%$ ). The larger rms variations of the line in-

indices measured from the TNG/HARPS-N spectra compared to the HET/HRS spectra measurements might be a consequence of the lower SNR of the TNG/HARPS-N spectra (40–70), compared to that of the HET/HRS spectra (120–220). There is no correlation between neither HET/HRS  $I_{H\alpha,HRS}$  and RVs (the Pearson coefficient,  $r = 0.27$ ), nor between TNG/HARPS-N  $I_{H\alpha,HARPS-N}$  and RVs, (the same value of  $r = 0.27$ ). There is no any significant signal in the Lomb-Scargle periodograms of BD+03 2562  $H\alpha$  indices.

### 2.3.2. HD 103485

The iodine flat-field HET/HRS spectra of HD 103485 show marginal rms variations ( $I_{I_2,H\alpha} = 0.1\%$  and  $I_{I_2,Fe} = 0.13\%$ ) in the  $H\alpha$  and Fe I 6593.883 Å indices. Comparing to the relative scatter of  $H\alpha$  and Fe I indices ( $I_{H\alpha,HRS} = 3.16\%$  and  $I_{Fe,HRS} = 0.79\%$ ) we are assured of the negligible contribution of the weak iodine lines to  $H\alpha$  and Fe I 6593.883 Å line indices. The Pearson coefficient between HET/HRS  $H\alpha$  index and RVs is  $r = 0.11$ . The rms variations of  $H\alpha$  and Fe I 6593.883 Å line indices measured from 18 TNG/HARPS-N spectra are similar to those measured for BD+03 2562:  $I_{H\alpha,HARPS-N} = 3.86\%$  and  $I_{Fe,HARPS-N} = 2.73\%$ . However, the Pearson coefficient between TNG/HARPS-N  $H\alpha$  index and RVs,  $r = 0.66$ , while the critical value of the Pearson correlation coefficient at the confidence level of 0.01,  $r_{16,0.01} = 0.59$ . On the other hand, this value ( $r = 0.66$ ) is lower than the critical value of the Pearson correlation coefficient at the confidence level of 0.001 ( $r_{16,0.001} = 0.71$ ). Given the small number of epochs the correlation may very well be spurious. The  $H\alpha$  indices versus HET/HRS and TNG/HARPS-N radial velocities are presented on Figure 1. Figure 2 presents the TNG/HARPS-N radial velocity and  $H\alpha$  activity index curves of HD 103485. Figure 3 presents LS periodograms of TNG/HARPS-N and HET/HRS radial velocities and  $H\alpha$  indices.

### 2.4. Wavelength dependence of the radial velocity signal

As both HD 103485 and BD+03 2562 exhibit significant scatter both in radial velocities and  $H\alpha$  activity indices, the unambiguous interpretation of their origin is very difficult. Therefore, we analysed the wavelength dependence of the radial velocity peak-to-peak amplitude ( $A$ ). The value of  $A$  should be constant in the case of spectral shifts induced by the gravitational pull of the companion. In the case of a RV signal generated by the rotation of a spotted stellar photosphere, the value of  $A$  should decrease with increasing wavelength as the temperature difference between the stellar photosphere and a stellar spot decreases at longer wavelengths (see e.g. Saar & Donahue 1997; Hatzes 2002; Desort et al. 2007).

Figure 4 shows,  $A$ , the peak-to-peak RV amplitude as a function of the TNG/HARPS-N order number for HD 103485, BD+03 2562, and the multiple planetary host PTPS target TYC 1422-00614-1 presented in Niedzielski et al. (2015b) (TAPAS-I paper). TYC 1422-00614-1 does not show any significant stellar activity related to any of the two signals reported in its radial velocity curve. Therefore, it is a good benchmark to test the wavelength dependence of the radial velocity signal peak-to-peak amplitudes of the stars in this paper HD 103485 and BD+03 2562. As shown in Figure 4, both HD 103485 and BD+03 2562 show chromatic dependence of  $A$ , although its unambiguous interpretation is not straightforward, especially if we note that the peak-

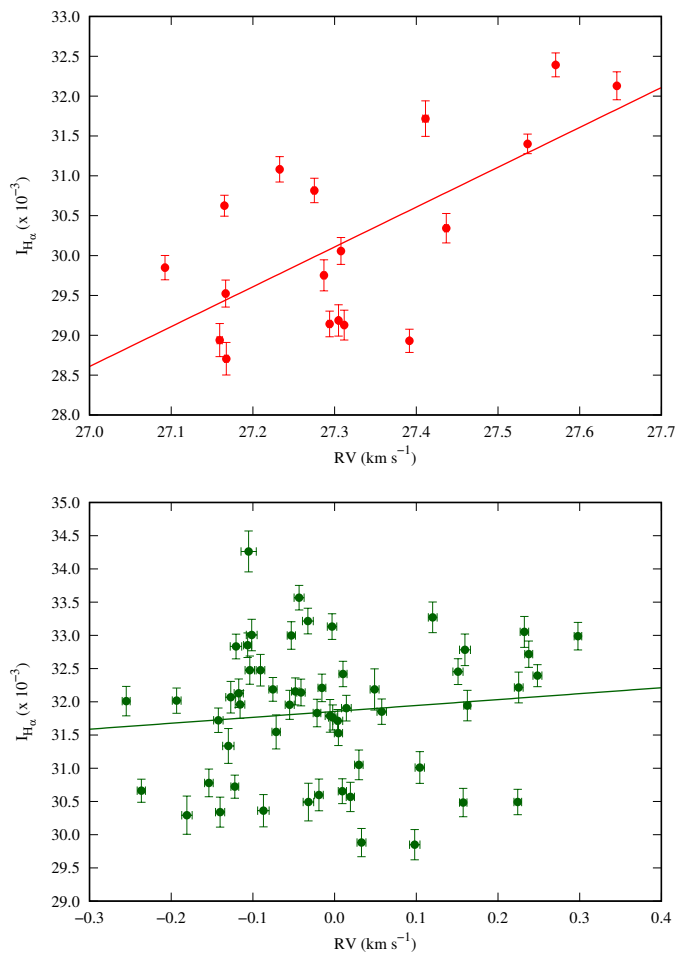


**Fig. 1.**  $H\alpha$  activity index of HD 103485 measured from TNG/HARPS-N spectra (top panel) and from HET/HRS ones (lower panel). Solid lines presents linear fits to the data. Although  $H\alpha$  activity index measured from HET/HRS does not present correlation with HET/HRS radial velocities, the one measured from TNG/HARPS-N spectra shows clear correlation with TNG/HARPS-N radial velocities.

to-peak RV amplitude is systematically higher in TNG/HARPS-N orders 10–16.

Equation (5) of Desort et al. (2007) gives the relation between the peak-to-peak amplitude of the RV variation ( $A$ ), the projected rotation velocity of the star ( $v_{\text{rot}} \sin i_{\star}$ ) and the fraction of the visible hemisphere of the star that might be covered by the spot (parameter  $f_r$ , see Desort et al. 2007 for its definition and relation to the fraction of the projected area covered by the spot,  $f_p$ , on the 2D stellar disk used by other authors). Using the above mentioned equation we computed the parameter  $f_r$  for HD 103485 and BD+03 2562. As inputs in equation (5) we used the values of the projected rotation velocities of both stars from Tables 1 and 2 and the values of the  $K$  semi-amplitudes from Tables 3 and 4 ( $A$  is  $\approx 2K$ ). For HD 103485 we obtained  $f_r = 5.93\%$  and for BD+03 2562  $f_r = 5.71\%$ . Then, using equation (6) of Desort et al. (2007), that gives the relation between the peak-to-peak amplitude of the bisector inverse slope peak-to-peak variation ( $S$ ), the parameter  $f_r$ ,  $v_{\text{rot}} \sin i_{\star}$  and the instrumental width of the spectrograph ( $v_0 = 3 \text{ km s}^{-1}$  for both HARPS and HARPS-N) we computed the values of  $S$  for both of our targets. We obtain  $S = 96 \text{ m s}^{-1}$  for HD 103485 and  $S = 75.5 \text{ m s}^{-1}$  for BD+03 2562. The computed value of the peak-to-peak amplitude of bisector inverse slope for HD 103485 is consis-

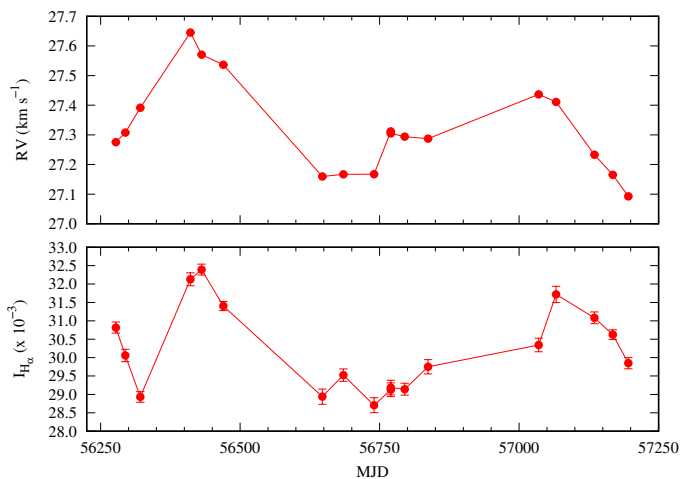


**Fig. 2.** The TNG/HARPS-N radial velocity and H $\alpha$  activity index curves of HD 103485.

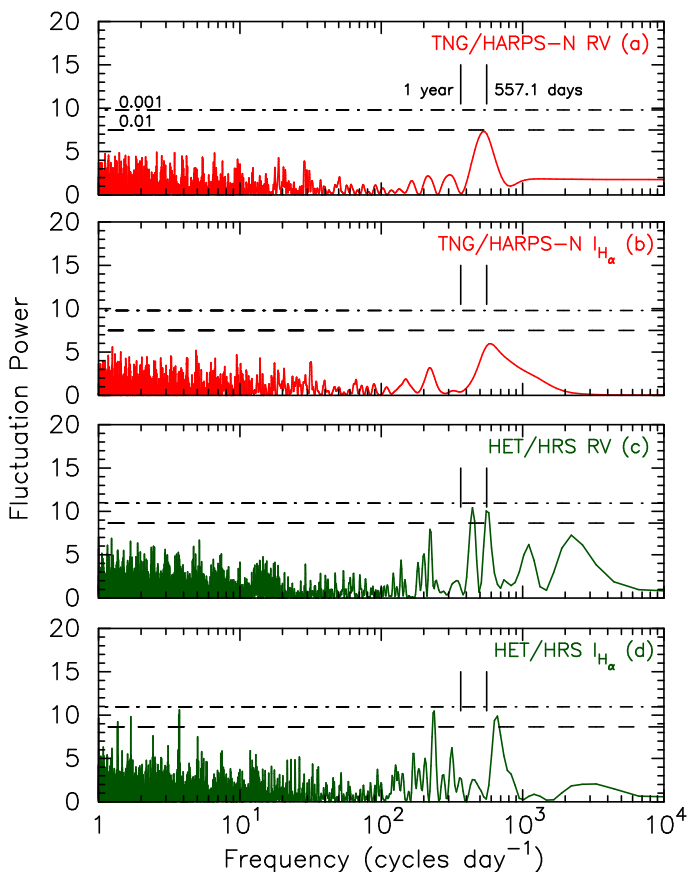


**Fig. 3.** LS periodograms of (a) TNG/HARPS-N RVs, (b) TNG/HARPS-N H $\alpha$  activity index, (c) HET/HRS RVs, and (d) HET/HRS H $\alpha$  activity index of HD 103485. The levels of FAP = 1.0% and 0.1% are shown.

tent with its peak-to-peak amplitude of TNG/HARPS-N BIS ( $85 \text{ m s}^{-1}$ , see section 2.1.), while in the case of BD+03 2562, it is significantly higher (see section 2.1. TNG/HARPS-N BIS for BD+03 2562 is  $58 \text{ m s}^{-1}$ ). We have to remember though, that equations (5) and (6) were derived for main sequence K5 type stars and HD 103458 and BD+03 2562 are giant stars.

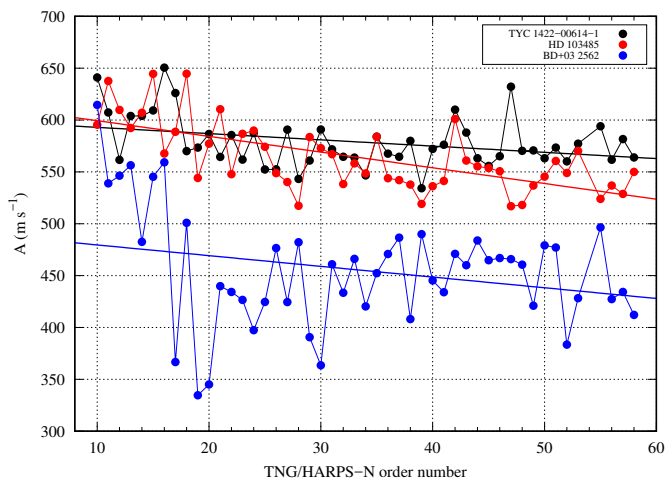


**Fig. 4.** Radial velocity peak-to-peak amplitude ( $A$ ) as a function of TNG/HARPS-N order number.

### 3. Stellar rotation and solar-like oscillations

The one sigma limit of the rotation period ( $P_{\text{rot}}(\sin i_{\star})^{-1}$ ) is equal to  $477 \pm 134$  days for HD 103485 and  $606 \pm 179$  days for BD+03 2562. Thus, the true rotation period ( $P_{\text{rot}}$ ) of HD 103485 at one sigma is then lower than 611 days and  $P_{\text{rot}}$  is lower than 785 days for BD+03 2562. Based on the upper limits of the rotation periods of HD 103485 and BD+03 2562 we then cannot exclude that the signals in their radial velocity curves are generated by rotational modulation of active photospheres.

The amplitudes ( $V_{\text{osc}}$ ) and periods ( $P_{\text{osc}}$ ) of solar-like oscillations computed using equations (7) and (10) of Kjeldsen & Bedding (1995) are equal to  $68.2^{+52.1}_{-28.2} \text{ m s}^{-1}$  and  $2.2^{+2.0}_{-1.1}$  days for HD 103485 and to  $102.9^{+89.9}_{-45.4} \text{ m s}^{-1}$  and  $2.9^{+3.2}_{-1.7}$  days for BD+03 2562. Computed values of solar-like oscillations amplitudes are consistent with the values of stellar jitter ( $\sigma_{\text{jitter}}$ ) and post-fit rms (RMS) presented in Tables 3 and 4. Both stars exhibit extremely high stellar jitter.

### 4. Photometry and discussion of activity indicators

For HD 103485 two extensive sets of photometric observations are available from Hipparcos (Perryman et al. 1997; van Leeuwen 2007) and ASAS (Pojmanski 1997). 133 epochs of Hipparcos data were gathered over 1140 days between JD 2447878.4 and 2449019.0, long before our monitoring of this star. The average brightness is  $v_{\text{Hip}} = 8.422 \pm 0.013$  mag and they show no trace of variability. 392 epochs of ASAS photometry were collected between JD 2451871.9 and 2455040.5 (3169 days), partly during our HET observations. These show average brightness of  $v_{\text{ASAS}} = 8.281 \pm 0.01$  and trace of a 27d period, possibly due to the Moon. No significant photometric variability similar to that shown in RV is present in the available data as illustrated by the LS periodogram in Figure 6.

BD+03 2562 was observed within ASAS over 3169 days between JD 2451871.9 and 2455040.5, partly covering the timespan of our HET observations. The average brightness is  $v_{\text{ASAS}} = 9.497 \pm 0.015$  mag and we find no trace of activity in these data (see Figure 8).

The spectral line bisectors and the calcium H&K line shape show that we are dealing with a Keplerian motion that alters the position of the observed absorption lines in the spectra of both stars. Both weak and uncorrelated variations of H $\alpha$  and the lack

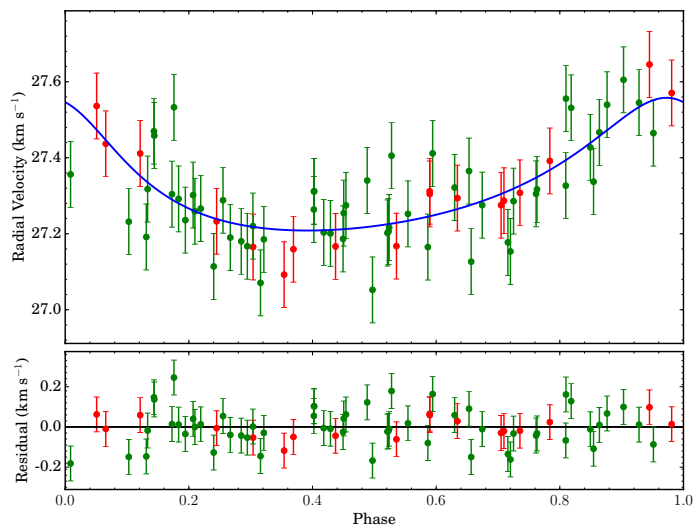


**Fig. 5.** Keplerian best fit to combined HET HRS (green points) and TNG HARPS-N (red points) data for HD 103485. The estimated jitter due to p-mode oscillations has been added to the uncertainties.

of photometric variability in the case of BD+03 2562 support that conclusion. In the case of HD 103485 the  $H\alpha$  variations, weakly correlated with the observed RV in the TNG/HARPS-N data suggest that the observed RV variations may be due to a spot, but no such spot is visible in the photometric data, partly contemporaneous with our spectroscopic observations.

We can therefore conclude that, although in the case of HD 103485 the activity should be studied in more detail in the future, there exists no inexorable evidence that contradicts the interpretation of the observed RV variations as Doppler displacements due to the presence of a companion.

## 5. Keplerian analysis

The Keplerian orbital parameters have been derived using a hybrid approach (e.g. Goździewski et al. 2003; Goździewski & Migaszewski 2006; Goździewski et al. 2007), in which the PIKAIA-based, global genetic algorithm (GA; Charbonneau 1995) was combined with the MPPFIT algorithm (Markwardt 2009), to find the best-fit Keplerian orbit delivered by RVLIN (Wright & Howard 2009) modified to allow the stellar jitter to be fitted as a free parameter (Ford & Gregory 2007; Johnson et al. 2011). The RV bootstrapping method (Murdoch et al. 1993; Kuerster et al. 1997; Marcy et al. 2005; Wright et al. 2007) is employed to assess the uncertainties of the best-fit orbital parameters (see TAPAS I for more details). The results of the Keplerian analysis for HD 103485 are presented in Table 3 and in Figure 5 and for BD+03 2562 in Table 4 and in Figure 7.

## 6. Discussion and conclusions

In this paper, the fifth of our TAPAS series, we present a planetary mass companion and a possible one to two very metal poor giant stars in the constellation of Virgo. We have interpreted the RV variations measured in both stars as Keplerian motion, and while there is a lack of compelling evidence that the signal is originated by stellar activity for BD+03 2562 it is not so clear for HD 103485 for which based on the available data both interpretations for the RV signal (planet and activity) are possible. In the meanwhile more data is gathered for HD 103485 it

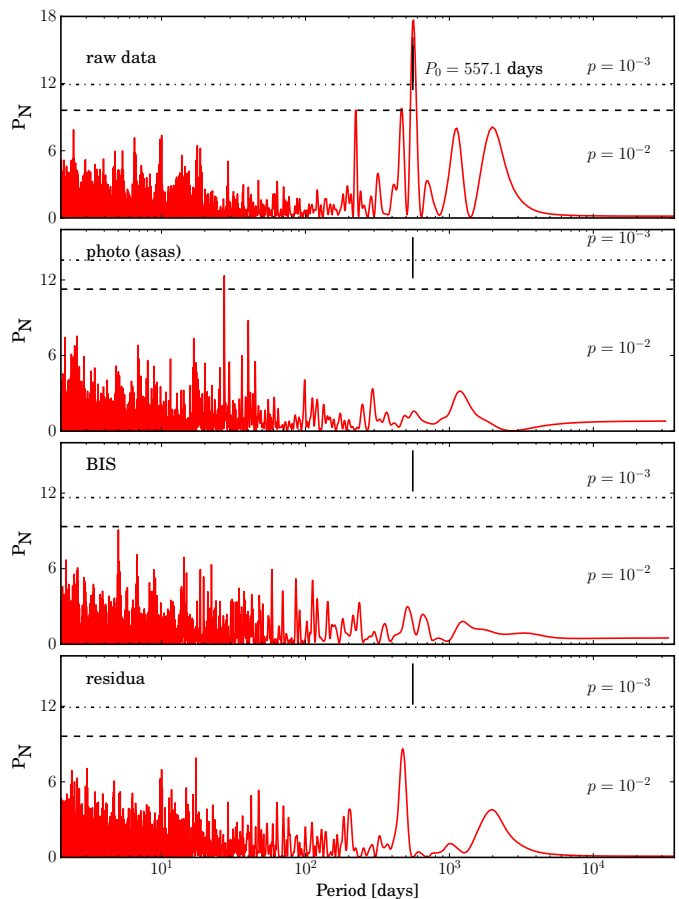


**Fig. 6.** From top to bottom Lomb-Scargle periodograms for (a) the original HET HRS and HARPS-N RV data of HD 103485, (b) ASAS photometry, (c) Bisector analysis, and (d) RV residua (HET and TNG) after the best Keplerian planet fit.

is hard to justify or disprove both possible interpretations so we keep as a working hypothesis for the following discussion that the RV signal is originated by a planet. In this case, both giant stars have masses close to Solar ( $1.11 M_{\odot}$  HD 103485 and  $1.14 M_{\odot}$  BD+03 2562), very low metallicities ( $[Fe/H] = -0.50$  and  $-0.71$  for HD 103485 and BD+03 2562 respectively) and Jupiter planetary mass companions ( $m_2 \sin i = 7$  and  $6.4 M_J$  for HD 103485 and BD+03 2562 resp.) in close to terrestrial orbits (1.4 au HD 103485 and 1.3 au BD+03 2562) with moderate eccentricities ( $e = 0.34$  and  $0.2$  for HD 103485 and BD+03 2562).

In Fig. 9 we show the location of all the stars included in the PTPS sample on the Hertzsprung-Russell (HR) diagram where we have marked the location of HD 103485 (blue) and BD+03 2562 (red) (and their corresponding uncertainties). The Bertelli et al. (2008) evolutionary tracks of a  $1 M_{\odot}$  stars at two different very low metallicities are also shown for comparison. From the figure is clear that the two stars presented in this paper are among the most evolved stars of the whole PTPS sample. With ages of 6.17 and 5.25 Gyr for HD 103485 and BD+03 2562 (see Tables 1 and 2), these stars are certainly above the mean age value of 3.37 Gyr obtained for Giant stars with planets in Maldonado & Villaver (2016).

Again under the interpretation that the RV signal measured in both stars is due to Keplerian motion and based on the derived orbital parameters we compute the orbital solution under stellar evolution. None of the planets are expected to have

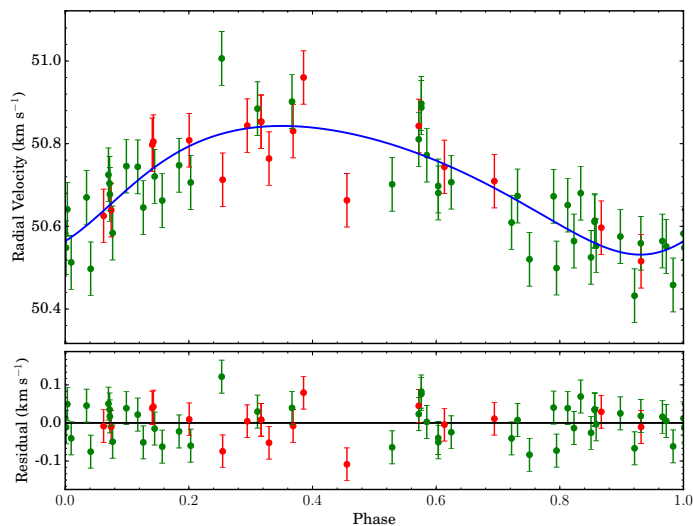


**Fig. 7.** Keplerian best fit to combined HET HRS and TNG HARPS-N data for BD+03 2562. The jitter is added to the uncertainties.

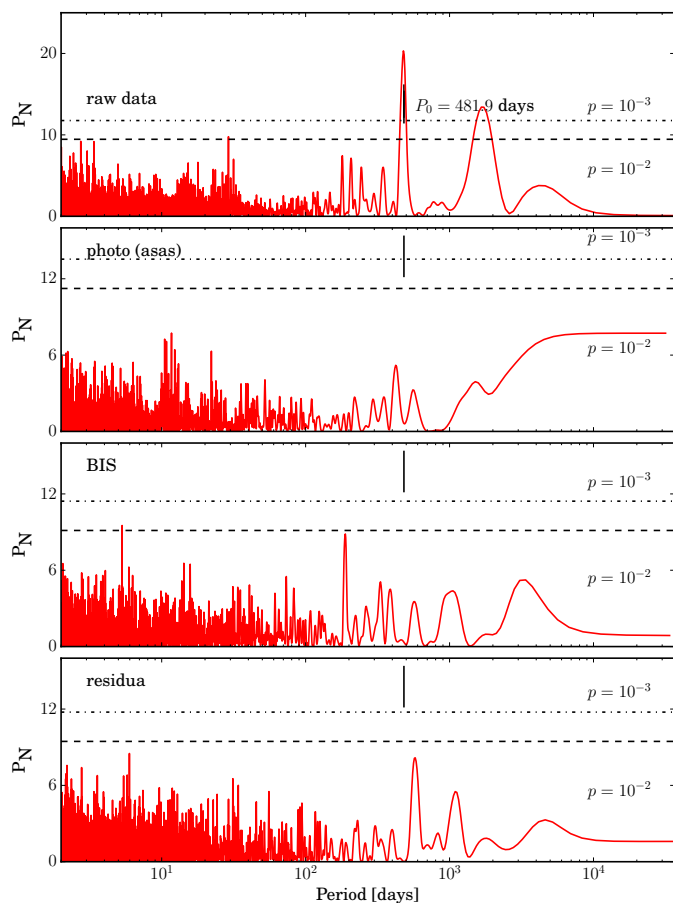


**Fig. 8.** Same as Fig.6 for BD+03 2562

experienced orbital decay caused by stellar tides at their current location (with  $a/R_\star = 10.99$  and  $8.64$  for HD 103485 and BD+03 2562 respectively) (see e.g. Villaver & Livio 2009; Villaver et al. 2014). Given the tidal dissipation mode that operates in these giant stars, the planets should experience eccentricity decay together with orbital decay (Villaver et al. 2014), thus their moderate eccentricities and their  $a/R_\star$  ratios are con-

**Table 3.** Keplerian orbital parameters of HD 103485

| Parameter                                      | HD 103485               |
|--|-------------------------|
| $P$ (days)                                     | $557.1^{+5.0}_{-4.5}$   |
| $T_0$ (MJD)                                    | $53656^{+32}_{-35}$     |
| $K$ ( $\text{m s}^{-1}$ )                      | $175^{+16}_{-15}$       |
| $e$  | $0.34^{+0.16}_{-0.08}$  |
| $\omega$ (deg)                                 | $21^{+50}_{-50}$        |
| $m_2 \sin i$ ( $M_J$ )                         | $7 \pm 2$               |
| $a$ (au)                                       | $1.4 \pm 0.1$           |
| $V_0$ ( $\text{m s}^{-1}$ )                    | $27328.2^{+5.0}_{-5.2}$ |
| offset ( $\text{m s}^{-1}$ )                   | $27307^{+26}_{-27}$     |
| $\sigma_{\text{jitter}}$ ( $\text{m s}^{-1}$ ) | 86.6                    |
| $\sqrt{\chi^2_{\nu}}$                          | 1.05                    |
| RMS ( $\text{m s}^{-1}$ )                      | 88.3                    |
| $N_{\text{obs}}$                               | 75                      |

**Notes.**  $V_0$  denotes absolute velocity of the barycenter of the system, offset is a shift in radial velocity measurements between different telescopes,  $\sigma_{\text{jitter}}$  is stellar intrinsic jitter as defined in Johnson et al. (2011), RMS is the root mean square of the residuals.

**Table 4.** Keplerian orbital parameters of BD+03 2562

| Parameter                                      | BD+03 2562             |
|--|------------------------|
| $P$ (days)                                     | $481.9^{+2.7}_{-2.8}$  |
| $T_0$ (MJD)                                    | $53726^{+41}_{-32}$    |
| $K$ ( $\text{m s}^{-1}$ )                      | $155.7^{+1.0}_{-3.3}$  |
| $e$  | $0.20^{+0.12}_{-0.08}$ |
| $\omega$ (deg)                                 | $218^{+32}_{-26}$      |
| $m_2 \sin i$ ( $M_J$ )                         | $6.4 \pm 1.3$          |
| $a$ (au)                                       | $1.3 \pm 0.1$          |
| $V_0$ ( $\text{m s}^{-1}$ )                    | $50712^{+7}_{-5}$      |
| offset ( $\text{m s}^{-1}$ )                   | $50648^{+24}_{-24}$    |
| $\sigma_{\text{jitter}}$ ( $\text{m s}^{-1}$ ) | 64.7                   |
| $\sqrt{\chi^2_{\nu}}$                          | 1.11                   |
| RMS ( $\text{m s}^{-1}$ )                      | 69.8                   |
| $N_{\text{obs}}$                               | 64                     |

**Notes.**  $V_0$  denotes absolute velocity of the barycenter of the system, offset is a shift in radial velocity measurements between different telescopes,  $\sigma_{\text{jitter}}$  is stellar intrinsic jitter as defined in Johnson et al. (2011), RMS is the root mean square of the residuals.

sistent with both planets being yet too far from the star to have experienced tidal forces. Both planets reported in this paper are located in similar regions in  $M_\star$  versus orbital distance or the  $a - e$  plane as most of the other planets orbiting giant stars reported in the literature (Villaver et al. 2014). Neither HD 103485 b nor BD+03 2562 b, are expected to survive engulfment when the star evolves up the tip of the RGB (Villaver & Livio 2009). Assuming an average value of  $\sin i$  both these companions stay within the planetary-mass range.

Thus the orbital characteristics of the substellar object and the possible one we report in this paper do not appear to be differ-

ent from the ones shown by the bulk population of planets found orbiting giant or subgiant stars. These two objects, however, clearly stand out in two important aspects: i) they are among the few very massive planets found around metal poor stars, and ii) BD+03 2562 in particular populates a region in the  $M_\star - [\text{Fe}/\text{H}]_\star$  plane where only another star has been found to host planets BD+20 2457 (see Figs. 10 and 11).

From Figs. 10, 11 it is clear that the two planet/star combinations reported in this paper are very special. First, they are two of the very few massive planets orbiting around stars close to the mass of the Sun to be found at very low metallicity. At lower metallicities than BD+03 2562, only two other planets have been reported in the literature orbiting the stars BD+20 2457 (Niedzielski et al. 2009) and HD 11755 (Lee et al. 2015). The similarities among these systems are striking: giant, close to Solar mass, evolved stars with radii close to  $30 R_\odot$ , with  $\approx 7 M_J$  minimum mass planets and in  $\approx 1 \text{ au}$  orbits. Note also that the planet around HD 103485 is the only massive planet in the region around stars with metallicity in the range  $-0.6 < [\text{Fe}/\text{H}]_\star < -0.4$ . HD 103485 and BD+03 2562 stand out even more in Fig. 11 where very few planets are known with  $[\text{Fe}/\text{H}]_\star < -0.48$  and  $M_\star > 1 M_\odot$ .

Our current understanding of massive planet formation offers two channels. First, core accretion – and the growing of planets from the accretion of a gas envelope into a massive core – has problems to easily explain systems formed at low metallicity. Models of planet formation by core accretion require a protoplanetary disk with a high density of solids to form planetary cores which accrete gas before the primordial gas disk dissipates (see Ida & Lin 2004). The probability of a star hosting a planet that is detectable in radial velocity surveys increases  $P_{pl}(Z) = 0.03 \times 10^{2 \times Z}$ , where  $Z = [\text{Fe}/\text{H}]$  is the stellar metallicity between  $-0.5$  and  $0.5$  dex (Gonzalez 1997; Fischer & Valenti 2005). Thus although, core accretion does not exclude the formation at low metallicity, the probability of finding such planets is low  $P_{pl} = 0.2\%$  for HD 103485 and  $0.1\%$  for BD+03 2562.

The alternative mechanism, in-situ fragmentation via gravitational instability (GI) (see e.g., Cameron 1978; Boss 1997) poses such strong requirements in the characteristics of a protoplanetary disk at 1 au that has been shown cannot exist on dynamical grounds (see e.g. Rafikov 2005; Stamatellos & Whitworth 2008). The planet could form by GI at larger distances (Rafikov 2005; Matzner & Levin 2005) and experience subsequent migration to  $\approx 400d$  orbital periods in relatively short timescales. In fact, the fragments formed by instability at 100 au are expected to have minimum masses of  $10 M_J$  (Rafikov 2005) which is approximately the typical mass of the planets found around the low metallicity stars reported in this paper. Note that although it has been shown that GI cannot be the main channel for planet formation as it cannot reproduce the overall characteristics of the bulk of the planet detections, nothing prevents it to be the preferred mechanism under certain circumstances. In fact, it has been reported that protoplanetary disks with low metallicities generally cool faster and show stronger overall GI activity (Mejía et al. 2005; Cai et al. 2006) although the lowest metallicity considered in these models is a quarter Solar (still much larger than the ones shown by the stars presented in this paper). So the question still remains on how gas cooling in the disk operates at the low metallicity of these stars given the disk needs to be atypically cold for GI and whether these planets represent indeed the low-mass tail of the distribution of disk-born companions (Kratter et al. 2010).

Planet host giants, in fact, have been reported to show peculiar characteristics regarding the planet-metallicity relation. In particular, Maldonado et al. (2013) show that, whilst the

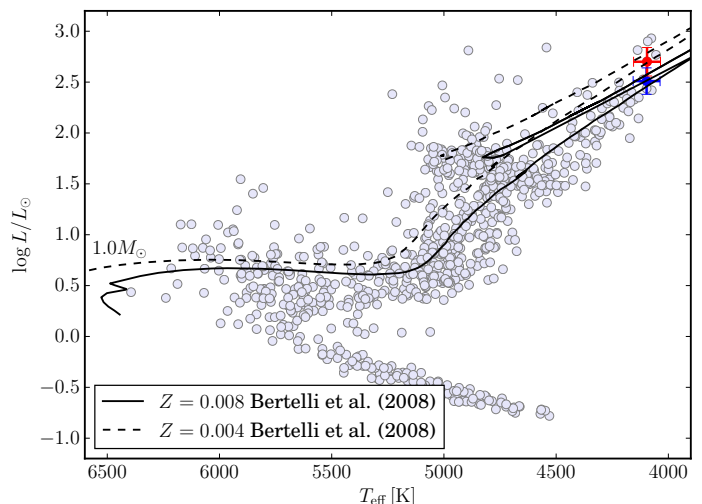


**Fig. 9.** Hertzsprung-Russell diagram for the complete PTPS sample with HD 103485 (in blue) and BD+03 2562 (in red) and the evolutionary tracks from Bertelli et al. (2008) for a star with  $1 M_\odot$  and metallicities  $Z = 0.008$  and  $Z = 0.004$  (see the legend in the bottom left corner of the plot).

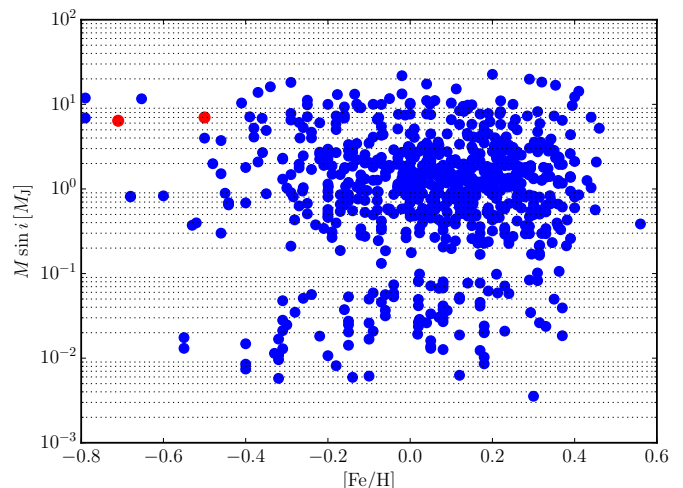


**Fig. 10.** Planet minimum mass ( $M \sin i$  in Jupiter mass) versus stellar metallicity ( $[\text{Fe}/\text{H}]$ ) for all the confirmed planets (blue points) as taken from the Exoplanet encyclopedia (exoplanet.eu, exoplanets.org). The two red points represent the location of the planets reported in this paper. The horizontal lines are to guide the eye in the logarithmic scale in the vertical axis.

metallicity distribution of planet-hosting giant stars with stellar masses  $M > 1.5 M_\odot$  follows the general trend that has been established for main sequence stars hosting planets, giant planet hosts in the mass domain  $M \leq 1.5 M_\odot$  do not show metal enrichment. Similar results were found by Mortier et al. (2013). Note that Reffert et al. (2015) challenged these results based on a discussion of planet contamination but it has been shown by Maldonado & Villaver (2016) based on their planet list that the result is sustained using the Reffert et al. (2015) list of candidates.

The two objects presented in this paper add two more points to a already puzzling relation between giant planets and giant stars that might help understand planet formation mechanisms for low metallicity stars.

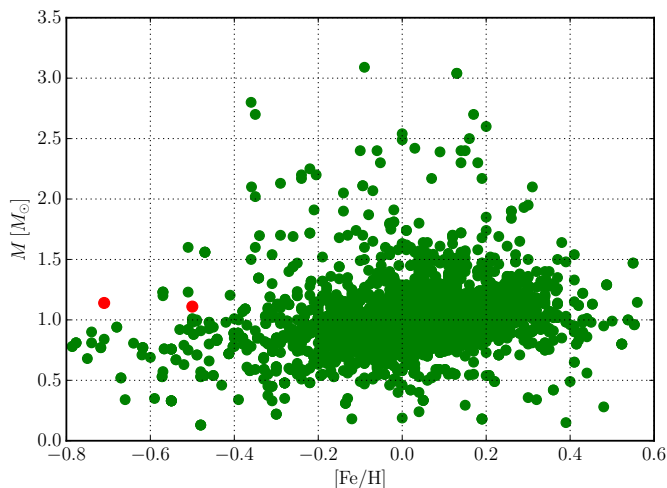


**Fig. 11.** Stellar mass (in  $M_{\odot}$ ) versus stellar metallicity ([Fe/H]) for all the stars with confirmed planets (green points) according to the Exoplanet encyclopedia (exoplanet.eu, exoplanets.org). The two red points represent the location of the stars reported in this paper.

**Acknowledgements.** We thank the HET and IAC resident astronomers and telescope operators for their support. EV acknowledges support from the Spanish Ministerio de Economía y Competitividad under grant AYA2014-55840P. MA acknowledges the Mobility+III fellowship from the Polish Ministry of Science and Higher Education. AN, BD-S and MiA were supported by the Polish National Science Centre grant no. UMO-2012/07/B/ST9/04415 and UMO-2015/19/B/ST9/02937. KK was funded in part by the Gordon and Betty Moore Foundation's Data-Driven Discovery Initiative through Grant GBMF4561. This research was supported in part by PL-Grid Infrastructure. The HET is a joint project of the University of Texas at Austin, the Pennsylvania State University, Stanford University, Ludwig-Maximilians-Universität München, and Georg-August-Universität Göttingen. The HET is named in honor of its principal benefactors, William P. Hobby and Robert E. Eberly. The Center for Exoplanets and Habitable Worlds is supported by the Pennsylvania State University, the Eberly College of Science, and the Pennsylvania Space Grant Consortium. This work made use of NumPy (Walt et al. 2011), Matplotlib (Hunter 2007), Pandas (McKinney 2010) and yt (Turk et al. 2011) and of the Exoplanet Orbit Database and the ExoplanetData Explorer at exoplanets.org and exoplanet.eu.

## References

- Adamczyk, M., Deka-Szymankiewicz, B., & Niedzielski, A. 2016, *A&A*, 587, A119
- Adamów, M., Niedzielski, A., Villaver, E., Wolszczan, A., & Nowak, G. 2014, *A&A*, 569, A55
- Adamów, M., M., Niedzielski, A., Villaver, E., et al. 2015, *A&A*, 581, A94
- Baranne, A., Mayor, M., & Poncet, J. L. 1979, *Vistas in Astronomy*, 23, 279
- Baranne, A., Queloz, D., Mayor, M., et al. 1996, *A&AS*, 119, 373
- Bertelli, G., Girardi, L., Marigo, P., & Nasi, E. 2008, *A&A*, 484, 815
- Boss, A. P. 1997, *Science*, 276, 1836
- Boss, A. P. 2004, *ApJ*, 610, 456
- Butler, R. P., Marcy, G. W., Williams, E., et al. 1996, *PASP*, 108, 500
- Cai, K., Durisen, R. H., Michael, S., et al. 2006, *ApJ*, 636, L149
- Cameron, A. G. W. 1978, *Moon and Planets*, 18, 5
- Charbonneau, P. 1995, *ApJS*, 101, 309
- Cincunegui, C., Díaz, R. F., & Mauas, P. J. D. 2007, *A&A*, 469, 309
- Cosentino, R., Lovis, C., Pepe, F., et al. 2012, in *SPIE Conference Series*, Vol. 8446, *SPIE Conference Series*
- da Silva, L., Girardi, L., Pasquini, L., et al. 2006, *A&A*, 458, 609
- Desort, M., Lagrange, A.-M., Galland, F., Udry, S., & Mayor, M. 2007, *A&A*, 473, 983
- Duncan, D. K., Vaughan, A. H., Wilson, O. C., et al. 1991, *ApJS*, 76, 383
- Eberhard, G. & Schwarzschild, K. 1913, *ApJ*, 38, 292
- Fellgett, P. 1955, *Optica Acta*, 2, 9
- Figueira, P., Faria, J. P., Adibekyan, V. Z., Oshagh, M., & Santos, N. C. 2016, *Origins of Life and Evolution of the Biosphere*, 46, 385
- Fischer, D. A. & Valenti, J. 2005, *ApJ*, 622, 1102
- Ford, E. B. & Gregory, P. C. 2007, in *ASP Conference Series*, Vol. 371, *Statistical Challenges in Modern Astronomy IV*, ed. G. J. Babu & E. D. Feigelson, 189
- Ghezzi, L., Cunha, K., Schuler, S. C., & Smith, V. V. 2010, *ApJ*, 725, 721
- Gomes da Silva, J., Santos, N. C., Bonfils, X., et al. 2012, *A&A*, 541, A9
- Gonzalez, G. 1997, *MNRAS*, 285, 403
- Goździewski, K., Konacki, M., & Maciejewski, A. J. 2003, *ApJ*, 594, 1019
- Goździewski, K., Maciejewski, A. J., & Migaszewski, C. 2007, *ApJ*, 657, 546
- Goździewski, K. & Migaszewski, C. 2006, *A&A*, 449, 1219
- Griffin, R. F. 1967, *ApJ*, 148, 465
- Hatzes, A. P. 2002, *Astronomische Nachrichten*, 323, 392
- Høg, E., Fabricius, C., Makarov, V. V., et al. 2000, *A&A*, 355, L27
- Hunter, J. D. 2007, *Computing In Science & Engineering*, 9, 90
- Ida, S. & Lin, D. N. C. 2004, *ApJ*, 616, 567
- Jofré, E., Petrucci, R., Saffe, C., et al. 2015, *A&A*, 574, A50
- Johnson, J. A., Clanton, C., Howard, A. W., et al. 2011, *ApJS*, 197, 26
- Jones, M. I., Jenkins, J. S., Bluhm, P., Rojo, P., & Melo, C. H. F. 2014, *A&A*, 566, A113
- Kjeldsen, H. & Bedding, T. R. 1995, *A&A*, 293, 87
- Kratter, K. M., Murray-Clay, R. A., & Youdin, A. N. 2010, *ApJ*, 710, 1375
- Kuerster, M., Schmitt, J. H. M. M., Cutispoto, G., & Dennerl, K. 1997, *A&A*, 320, 831
- Lee, B.-C., Park, M.-G., Lee, S.-M., et al. 2015, *A&A*, 584, A79
- Lomb, N. R. 1976, *Ap&SS*, 39, 447
- Lovis, C., Dumusque, X., Santos, N. C., et al. 2011, *ArXiv e-prints* [arXiv:1107.5325]
- Maciejewski, G., Niedzielski, A., Wolszczan, A., et al. 2013, *AJ*, 146, 147
- Maldonado, J. & Villaver, E. 2016, *A&A*, 588, A98
- Maldonado, J., Villaver, E., & Eiroa, C. 2013, *A&A*, 554, A84
- Marcy, G. W. & Butler, R. P. 1992, *PASP*, 104, 270
- Marcy, G. W., Butler, R. P., Vogt, S. S., et al. 2005, *ApJ*, 619, 570
- Markwardt, C. B. 2009, in *Astronomical Society of the Pacific Conference Series*, Vol. 411, *Astronomical Data Analysis Software and Systems XVIII*, ed. D. A. Bohlender, D. Durand, & P. Dowler, 251
- Matzner, C. D. & Levin, Y. 2005, *ApJ*, 628, 817
- Mayer, L., Quinn, T., Wadsley, J., & Stadel, J. 2002, *Science*, 298, 1756
- Mayor, M. & Queloz, D. 1995, *Nature*, 378, 355
- McKinney, W. 2010, in *Proceedings of the 9th Python in Science Conference*, ed. S. van der Walt & J. Millman, 51 – 56
- Mejía, A. C., Durisen, R. H., Pickett, M. K., & Cai, K. 2005, *ApJ*, 619, 1098
- Mizuno, H. 1980, *Progress of Theoretical Physics*, 64, 544
- Mordasini, C., Alibert, Y., Benz, W., Klahr, H., & Henning, T. 2012, *A&A*, 541, A97
- Mortier, A., Santos, N. C., Sousa, S. G., et al. 2013, *A&A*, 557, A70
- Murdoch, K. A., Hearnshaw, J. B., & Clark, M. 1993, *ApJ*, 413, 349
- Mustill, A. J. & Villaver, E. 2012, *ApJ*, 761, 121
- Niedzielski, A., Deka-Szymankiewicz, B., Adamczyk, M., et al. 2016a, *A&A*, 585, A73
- Niedzielski, A., Konacki, M., Wolszczan, A., et al. 2007, *ApJ*, 669, 1354
- Niedzielski, A., Nowak, G., Adamów, M., & Wolszczan, A. 2009, *ApJ*, 707, 768
- Niedzielski, A., Villaver, E., Nowak, G., et al. 2016b, *A&A*, 588, A62
- Niedzielski, A., Villaver, E., Nowak, G., et al. 2016c, *A&A*, 589, L1
- Niedzielski, A., Villaver, E., Wolszczan, A., et al. 2015a, *A&A*, 573, A36
- Niedzielski, A., Villaver, E., Wolszczan, A., et al. 2015b, *A&A*, 573, A36
- Niedzielski, A. & Wolszczan, A. 2008, in *Astronomical Society of the Pacific Conference Series*, Vol. 398, *Extreme Solar Systems*, ed. D. Fischer, F. A. Rasio, S. E. Thorsett, & A. Wolszczan, 71
- Niedzielski, A., Wolszczan, A., Nowak, G., et al. 2015c, *ApJ*, 803, 1
- Nowak, G. 2012, PhD thesis, Nicolaus Copernicus Univ., Toruń, Poland
- Nowak, G., Niedzielski, A., Wolszczan, A., Adamów, M., & Maciejewski, G. 2013, *ApJ*, 770, 53
- Noyes, R. W., Hartmann, L. W., Baliunas, S. L., Duncan, D. K., & Vaughan, A. H. 1984, *ApJ*, 279, 763
- Pasquini, L., Döllinger, M. P., Weiss, A., et al. 2007, *A&A*, 473, 979
- Pepe, F., Mayor, M., Galland, F., et al. 2002, *A&A*, 388, 632
- Perri, F. & Cameron, A. G. W. 1974, *Icarus*, 22, 416
- Perryman, M. A. C., Lindgren, L., Kovalevsky, J., et al. 1997, *A&A*, 323, L49
- Pojmanski, G. 1997, *Acta Astron.*, 47, 467
- Pollack, J. B., Hubickyj, O., Bodenheimer, P., et al. 1996, *Icarus*, 124, 62
- Press, W. H., Teukolsky, S. A., Vetterling, W. T., & Flannery, B. P. 1992, *Numerical recipes in FORTRAN. The art of scientific computing* (Cambridge University Press)
- Privitera, G., Meynet, G., Eggenberger, P., et al. 2016a, *A&A*, 593, L15
- Privitera, G., Meynet, G., Eggenberger, P., et al. 2016b, *A&A*, 591, A45
- Privitera, G., Meynet, G., Eggenberger, P., et al. 2016c, *A&A*, 593, A128
- Queloz, D. 1995, in *IAU Symposium*, Vol. 167, *New Developments in Array Technology and Applications*, ed. A. G. D. Philip, K. Janes, & A. R. Uppgren, 221
- Rafikov, R. R. 2005, *ApJ*, 621, L69
- Ramsey, L. W., Adams, M. T., Barnes, T. G., et al. 1998, in *SPIE Conference Series*, Vol. 3352, *SPIE Conference Series*, ed. L. M. Stepp, 34–42

Reffert, S., Bergmann, C., Quirrenbach, A., Trifonov, T., & Künstler, A. 2015, A&A, 574, A116  
 Robertson, P., Endl, M., Cochran, W. D., & Dodson-Robinson, S. E. 2013, ApJ, 764, 3  
 Saar, S. H. & Donahue, R. A. 1997, ApJ, 485, 319  
 Santos, N. C., Israelian, G., & Mayor, M. 2004, A&A, 415, 1153  
 Scargle, J. D. 1982, ApJ, 263, 835  
 Shetrone, M., Cornell, M. E., Fowler, J. R., et al. 2007, PASP, 119, 556  
 Simon, J. B., Armitage, P. J., Li, R., & Youdin, A. N. 2016, ApJ, 822, 55  
 Stamatellos, D. & Whitworth, A. P. 2008, A&A, 480, 879  
 Tull, R. G. 1998, in SPIE Conference Series, Vol. 3355, SPIE Conference Series, ed. S. D'Odorico, 387–398  
 Turk, M. J., Smith, B. D., Oishi, J. S., et al. 2011, ApJS, 192, 9  
 Udry, S. & Santos, N. C. 2007, ARA&A, 45, 397  
 van Leeuwen, F. 2007, A&A, 474, 653  
 Villaver, E. & Livio, M. 2007, ApJ, 661, 1192  
 Villaver, E. & Livio, M. 2009, ApJ, 705, L81  
 Villaver, E., Livio, M., Mustill, A. J., & Siess, L. 2014, ApJ, 794, 3  
 Walt, S. v. d., Colbert, S. C., & Varoquaux, G. 2011, Computing in Science and Engg., 13, 22  
 Wright, J. T. & Howard, A. W. 2009, ApJS, 182, 205  
 Wright, J. T., Marcy, G. W., Fischer, D. A., et al. 2007, ApJ, 657, 533  
 Youdin, A. N. 2011, ApJ, 731, 99  
 Zieliński, P., Niedzielski, A., Wolszczan, A., Adamów, M., & Nowak, G. 2012, A&A, 547, A91

**Table 5.** HET and HRS RV and BIS measurements ( $\text{m s}^{-1}$ ) of HD 103485

| MJD          | RV      | $\sigma_{RV}$ | BIS    | $\sigma_{BIS}$ |
|--------------|---------|---------------|--------|----------------|
| 53023.396748 | 159.57  | 6.67          | 52.97  | 20.25          |
| 53349.497471 | -120.73 | 6.97          | 18.92  | 23.61          |
| 53389.521123 | -105.25 | 9.38          | 0.94   | 9.39           |
| 53390.398189 | -101.55 | 6.63          | 5.59   | 20.29          |
| 53713.504688 | -75.47  | 5.03          | 61.34  | 16.20          |
| 53730.469410 | 10.27   | 5.01          | 17.97  | 15.08          |
| 53736.450347 | 150.99  | 6.23          | 4.91   | 23.15          |
| 53752.421736 | -3.16   | 5.77          | 38.96  | 19.03          |
| 53758.387778 | -15.56  | 4.78          | 85.74  | 13.41          |
| 53764.472211 | -71.56  | 5.11          | 11.97  | 15.25          |
| 53771.468009 | -5.62   | 5.90          | 30.50  | 21.04          |
| 53778.334097 | -41.08  | 5.14          | 57.19  | 13.22          |
| 53798.402685 | -19.16  | 5.26          | 35.25  | 13.23          |
| 53820.327072 | -140.15 | 5.65          | 39.07  | 14.60          |
| 53825.333646 | -87.17  | 6.98          | 24.80  | 25.16          |
| 53832.184578 | -236.60 | 5.06          | 30.82  | 11.02          |
| 53835.190376 | -122.14 | 4.87          | 2.87   | 11.36          |
| 53889.142350 | -103.83 | 5.78          | 47.98  | 13.38          |
| 54080.494797 | -2.24   | 5.26          | -14.81 | 21.43          |
| 54107.425972 | 248.28  | 5.39          | -18.00 | 15.35          |
| 54129.379907 | 120.04  | 5.37          | 85.30  | 13.44          |
| 54144.454317 | 232.28  | 5.22          | 72.06  | 17.44          |
| 54159.302743 | 297.81  | 4.65          | 40.43  | 14.48          |
| 54173.254462 | 237.63  | 4.84          | 63.52  | 16.70          |
| 54186.212963 | 157.43  | 4.50          | 78.54  | 11.76          |
| 54218.127784 | 48.89   | 5.49          | 31.04  | 15.28          |
| 54437.514450 | 3.88    | 6.08          | -4.03  | 18.40          |
| 54437.520914 | 4.68    | 5.09          | 12.48  | 12.34          |
| 54485.392633 | 32.88   | 5.49          | 46.55  | 18.89          |
| 54507.337703 | 98.05   | 6.34          | -7.39  | 19.88          |
| 54544.358096 | 104.23  | 5.67          | 2.48   | 15.79          |
| 54564.184074 | 14.31   | 5.95          | 16.64  | 14.78          |
| 54577.150104 | 57.68   | 5.80          | 40.09  | 16.05          |
| 54612.164201 | -130.14 | 6.93          | 25.87  | 20.25          |
| 54843.425116 | -115.73 | 5.87          | -9.33  | 10.13          |
| 54868.351563 | 225.36  | 5.32          | 28.37  | 16.97          |
| 55171.525139 | -153.91 | 5.35          | 44.17  | 17.87          |
| 55195.453252 | 9.48    | 5.09          | 2.68   | 16.53          |
| 55221.392708 | 19.29   | 5.05          | 7.21   | 16.05          |
| 55246.422118 | 29.68   | 5.25          | 72.43  | 14.38          |
| 55551.487361 | -43.54  | 6.12          | 9.95   | 14.16          |
| 55566.435694 | -106.47 | 4.97          | -2.00  | 16.87          |
| 55578.398380 | -53.02  | 5.03          | 77.56  | 14.94          |
| 55580.392459 | -32.69  | 6.60          | 63.22  | 21.96          |
| 55604.322911 | -255.04 | 4.88          | 61.88  | 15.32          |
| 55619.301128 | -90.72  | 5.34          | 47.17  | 16.51          |
| 55636.263281 | -54.98  | 5.54          | 11.47  | 17.44          |
| 55654.195978 | -142.37 | 5.81          | 44.86  | 11.18          |
| 55693.220660 | -180.79 | 6.35          | 47.69  | 15.09          |
| 55703.188322 | -32.04  | 6.42          | 42.51  | 12.06          |
| 55964.447500 | 162.42  | 4.27          | 19.69  | 10.58          |
| 56001.356383 | -48.11  | 4.70          | 51.40  | 12.81          |
| 56018.315793 | -193.32 | 5.35          | 4.04   | 12.91          |
| 56033.268374 | -117.32 | 5.65          | 49.77  | 15.72          |
| 56043.131134 | -127.15 | 6.03          | 42.22  | 15.92          |
| 56288.476146 | -21.54  | 4.70          | 52.59  | 16.50          |
| 56340.424410 | 224.16  | 4.73          | 68.38  | 14.27          |

**Table 6.** TNG and HARPS-N RV and BIS measurements ( $\text{m s}^{-1}$ ) of HD 103485

| MJD          | RV       | $\sigma_{\text{RV}}$ | BIS    |
|--------------|----------|----------------------|--------|
| 56277.247179 | 27275.10 | 1.97                 | 157.38 |
| 56294.234787 | 27307.70 | 1.20                 | 198.41 |
| 56321.174370 | 27391.60 | 1.10                 | 186.65 |
| 56410.966775 | 27645.50 | 1.35                 | 197.62 |
| 56430.962559 | 27570.60 | 1.02                 | 210.71 |
| 56469.909044 | 27536.20 | 1.43                 | 209.60 |
| 56647.244692 | 27159.30 | 3.09                 | 185.54 |
| 56685.175862 | 27166.60 | 1.70                 | 192.14 |
| 56740.046309 | 27167.50 | 2.14                 | 226.24 |
| 56770.016852 | 27311.80 | 1.57                 | 209.44 |
| 56770.065133 | 27304.80 | 1.24                 | 206.05 |
| 56794.966883 | 27293.80 | 2.02                 | 221.75 |
| 56836.907914 | 27287.00 | 2.06                 | 229.18 |
| 57035.192541 | 27436.70 | 2.22                 | 234.18 |
| 57066.212695 | 27411.20 | 3.26                 | 240.97 |
| 57135.092065 | 27232.80 | 1.36                 | 220.46 |
| 57167.958789 | 27165.10 | 0.65                 | 242.70 |
| 57195.906134 | 27092.30 | 1.31                 | 213.33 |

**Table 7.** HET and HRS RV and BIS measurements ( $\text{m s}^{-1}$ ) of BD+03 2562

| MJD          | RV      | $\sigma_{\text{RV}}$ | BIS    | $\sigma_{\text{BIS}}$ |
|--------------|---------|----------------------|--------|-----------------------|
| 53037.367523 | 162.58  | 9.31                 | 59.79  | 25.13                 |
| 53039.337060 | 248.83  | 10.61                | 81.11  | 32.98                 |
| 53039.350613 | 239.24  | 11.03                | 57.66  | 29.48                 |
| 53341.515486 | 58.00   | 7.32                 | 38.91  | 12.23                 |
| 53759.367361 | 76.58   | 6.54                 | 40.39  | 18.48                 |
| 53773.326875 | 97.62   | 6.06                 | 39.61  | 22.59                 |
| 53801.268322 | 14.42   | 6.09                 | 47.88  | 19.55                 |
| 54127.490388 | 32.19   | 7.26                 | 70.01  | 24.44                 |
| 54138.338883 | -37.01  | 8.54                 | 61.44  | 20.41                 |
| 54138.450851 | -34.41  | 8.24                 | 86.82  | 22.30                 |
| 54158.399971 | -72.73  | 7.45                 | 38.77  | 26.63                 |
| 54174.364925 | -89.03  | 5.57                 | 41.44  | 17.05                 |
| 54191.197078 | -83.65  | 6.55                 | 55.70  | 16.84                 |
| 54194.174068 | -96.84  | 6.35                 | 39.17  | 20.00                 |
| 54208.265365 | -99.68  | 7.78                 | 55.13  | 22.80                 |
| 54209.261464 | -6.83   | 6.99                 | 46.65  | 26.47                 |
| 54212.253084 | -135.25 | 6.87                 | 45.89  | 24.86                 |
| 54224.223663 | 21.94   | 5.59                 | 64.43  | 18.52                 |
| 54242.173779 | 55.84   | 6.93                 | -40.03 | 21.22                 |
| 54264.123675 | 95.88   | 7.55                 | 31.74  | 20.84                 |
| 54462.444896 | 53.61   | 7.03                 | 30.05  | 23.78                 |
| 54498.347031 | 49.62   | 7.49                 | -7.74  | 25.73                 |
| 54498.467564 | 32.75   | 7.85                 | 36.94  | 26.35                 |
| 54560.185220 | 25.32   | 7.53                 | 18.94  | 24.50                 |
| 54604.187876 | -83.64  | 7.62                 | -12.55 | 21.49                 |
| 54811.497899 | 358.20  | 7.39                 | 14.09  | 26.62                 |
| 54839.418223 | 236.66  | 6.98                 | -0.96  | 13.58                 |
| 54866.333733 | 253.73  | 7.64                 | 85.91  | 28.11                 |
| 55171.502292 | -65.61  | 6.18                 | -3.30  | 22.57                 |
| 55208.423212 | -64.20  | 8.23                 | -7.78  | 38.24                 |
| 55232.342153 | -2.61   | 5.44                 | 45.44  | 17.90                 |
| 55260.257106 | 99.62   | 7.65                 | 45.93  | 22.58                 |
| 55554.472876 | -148.97 | 7.14                 | -43.34 | 29.10                 |
| 55581.385388 | -123.10 | 6.05                 | 3.91   | 21.40                 |
| 55585.369132 | -95.27  | 5.93                 | -46.36 | 20.95                 |
| 55615.289612 | -215.92 | 7.42                 | 45.46  | 17.89                 |
| 55645.354259 | -189.93 | 6.51                 | 28.50  | 21.04                 |
| 55673.272147 | -150.91 | 6.20                 | 50.51  | 17.87                 |
| 55688.233883 | 29.30   | 6.69                 | 41.05  | 20.16                 |
| 55723.130874 | 72.67   | 7.03                 | 40.59  | 19.77                 |
| 55954.374120 | 58.71   | 6.46                 | 31.59  | 22.22                 |
| 56001.366777 | -38.82  | 5.36                 | 23.81  | 14.44                 |
| 56015.332512 | -127.79 | 7.08                 | 41.77  | 20.97                 |
| 56034.152297 | 24.60   | 6.97                 | 57.35  | 16.39                 |
| 56045.120087 | 3.30    | 6.22                 | 66.61  | 16.64                 |
| 56417.215810 | 124.19  | 6.47                 | 90.08  | 21.60                 |

**Table 8.** TNG and HARPS-N RV and BIS measurements ( $\text{m s}^{-1}$ ) of BD+03 2562

| MJD          | RV       | $\sigma_{\text{RV}}$ | BIS    |
|--------------|----------|----------------------|--------|
| 56277.252412 | 50843.70 | 1.93                 | 140.84 |
| 56294.229018 | 50764.00 | 1.13                 | 176.94 |
| 56321.169034 | 50960.10 | 1.03                 | 190.92 |
| 56410.961652 | 50842.90 | 1.27                 | 148.93 |
| 56430.957199 | 50743.80 | 1.39                 | 155.83 |
| 56469.901805 | 50709.30 | 1.51                 | 162.17 |
| 56647.240508 | 50625.20 | 2.99                 | 133.03 |
| 56685.171295 | 50797.30 | 2.06                 | 136.22 |
| 56740.042885 | 50712.70 | 2.97                 | 163.36 |
| 56770.012446 | 50852.50 | 1.91                 | 157.46 |
| 56770.060731 | 50853.50 | 1.51                 | 154.18 |
| 56794.960756 | 50830.40 | 2.34                 | 169.21 |
| 56836.901346 | 50663.00 | 3.12                 | 173.94 |
| 57035.183363 | 50596.80 | 2.35                 | 183.76 |
| 57066.205983 | 50515.60 | 6.44                 | 132.81 |
| 57135.084365 | 50639.10 | 1.40                 | 182.09 |
| 57167.950415 | 50805.00 | 1.37                 | 161.54 |
| 57195.899321 | 50808.10 | 1.49                 | 151.10 |